IBRACON Structures and Materials Journal
Revista IBRACON de Estruturas e Materiais
ISSN 1983-4195 ismj.org

ORIGINAL ARTICLE

Seismic fragility assessment of a RC frame considering concentrated and distributed plasticity modelling

Avaliação sísmica em um pórtico de concreto armado considerando a modelagem com plasticidade concentrada e distribuída

Isabela Durci Rodrigues[a]
Gustavo Henrique Ferreira Cavalcante[b]
Eduardo Marques Vieira Pereira[b]
Luiz Carlos Marcos Vieira Júnior[b]
Abbie Liel[c]
Gustavo Henrique Siqueira[b]

[a]Universidade de São Paulo – USP, Escola de Engenharia de São Carlos, Departamento de Estruturas, São Carlos, SP, Brasil
[b]Universidade Estadual de Campinas – UNICAMP, Faculdade de Engenharia Civil, Arquitetura e Urbanismo, Departamento de Estruturas, Campinas, SP, Brasil
[c]University of Colorado – Civil, Environmental and Architectural Engineering, Boulder, Colorado, United States

Received 02 September 2022
Accepted 23 March 2023

Abstract: Researchers must decide on how they will model the non-linear material response in a Finite Element simulation to assess seismic vulnerability. This paper aims at giving an insight into these modelling decisions by comparing Fiber and Lumped Plasticity Finite Element Models in static and dynamic non-linear analysis in a RC frame. The methodology is based on the performance-based earthquake engineering to determine the expected damage on structures. The results indicate that both models are in good agreement with the static analysis, and when considering Extensive and Complete Damage Limit States on the dynamic analysis. The choice between them depends on the main goals of the research and resources available, since they have a significant difference in processing time.

Keywords: lumped plasticity model, fiber model, fragility functions.

Resumo: Pesquisadores devem decidir sobre como modelar a resposta não linear do material em uma simulação com Elementos Finitos para avaliar a vulnerabilidade sísmica. Esse trabalho pretende auxiliar nessa tomada de decisão ao comparar os modelos de Fibra e de Plasticidade Concentrada em Elementos Finitos em análises não lineares estáticas e dinâmicas de um pórtico em concreto armado. A metodologia é baseada na engenharia de desempenho sísmico (PBEE) para determinar o dano nas estruturas. Os resultados indicam que os dois modelos apresentam uma boa correspondência em uma análise estática, e ao considerar os Estados Limite de Dano Extensivo e Completo na análise dinâmica. A escolha entre os dois depende dos objetivos principais do pesquisador e dos recursos disponíveis, já que eles apresentam uma significativa diferença no tempo de processamento.

Palavras-chave: plasticidade concentrada, modelo de fibras, funções de fragilidade.

How to cite: I. D. Rodrigues, G. H. F. Cavalcante, E. M. V. Pereira, L. C. M. Vieira Júnior, A. Liel, and G. H. Siqueira, "Seismic fragility assessment of a RC frame considering concentrated and distributed plasticity modelling," *Rev. IBRACON Estrut. Mater.*, vol. 17, no. 1, e17105, 2024, https://doi.org/10.1590/S1983-41952024000100005

Corresponding author: Isabela Durci Rodrigues. E-mail: idrodrigues@usp.br
Financial support: Coordenação de Aperfeiçoamento de Pessoal de Nível Superior - Brasil (CAPES) - Finance Code 001; São Paulo Research Foundation (FAPESP) - Finance Code 2018/23304-9 and 2019/23304-9. The opinions, findings, and conclusions or recommendations expressed in this paper are those of the authors only and do not necessarily reflect the views of the sponsors or affiliates.
Conflict of interest: Nothing to declare.
Data Availability: The data that support the findings of this study are available from the corresponding author, IDR, upon reasonable request.

1 INTRODUCTION

Earthquakes represent a concern for several countries, since they have the potential to cause a great number of casualties and damages in structures. Brazil is a mid-plate country located in the South America tectonic plate, which is considered a stable region when compared to places near the boundaries of tectonic plates. For the sake of comparison, a seismic event of magnitude 5 occurs in Brazil once in five years on average, while in the Andean region an earthquake of this magnitude happens on average twice a week [1]. Even though Brazil is located inside a tectonic plate, it presents a considerable history of small to moderate earthquakes, also including two events with moment magnitude (M) higher than 6. Nievas et al. [2] presents a database of events in several parts of the world with M ranging from 4.0 to 5.5 in which damage or casualties have been reported on them. In Brazil, studies report damages occurred in the João Camara earthquake sequence, in Rio Grande do Norte state and Itacarambi earthquake, in the state of Minas Gerais [3], [4]. Such damages are explained in places with small to moderate hazards due to the definition of risk, which considers not only hazard, but also exposure, vulnerability and consequences. One should note, therefore, that a low hazard does not imply low seismic risk in a region [5], especially if buildings are not properly designed to withstand seismic loads.

In order to evaluate the risk of building damage and collapse, the concept of Performance-based earthquake engineering (PBEE) has been developed over the years [6]. According to Krawinkler [7], it corresponds to the design, evaluation and construction of structures whose performance under extreme loads responds to the needs and objectives of owners, users and the society. As a preliminary step, design professionals, owners and/or other stakeholders shall identify the desired building performance, and, as the design decisions are made, evaluate whether the final building can achieve the indicated performance. In order to assess its performance capability, it is necessary to conduct structural analyses to predict the building's response considering the earthquake hazard [8]. To evaluate damages and describe how structural and non-structural elements behave with seismic actions, one must relate the engineering parameters chosen to monitor the structure and the damage extent [9]. For that, fragility functions can be used, since they represent the conditional probability of exceedance of a limit state for several levels of ground shaking represented by an intensity measure (IM) or an engineering demand parameter (EDP) [10]. This paper uses the first definition of fragility function.

The assessment of performance capability is the core of PBEE, and it requires consideration of all important aspects of the design, such as sufficiently realistic modeling of strength, stiffness and mass irregularities, and component behavior under cyclic loads [7]. The model shall simulate the increase of structural damage and collapse when subjected to severe ground shaking. So the non-linear analysis model used must be able to identify the key deterioration and collapse modes [11]. Also, models must be accurate for relatively low-level and frequent ground-motions, as well as for high-level events [12].

From the several existing methods to simulate cyclic response on reinforced concrete buildings through a non-linear analysis, there are two main categories to represent the non-linear material response on a Finite Element simulation: distributed plasticity, which can be represented by fiber models, and concentrated (or lumped) plasticity models [13]. Fiber models can capture cracking behavior and the spread of plasticity throughout the element, and discretize the element cross-section, considering confined and unconfined concrete and different configurations for longitudinal reinforcement steel. However, it has an inherent limitation on its formulation that makes the simulation of the strain softening associated with rebar buckling difficult [11]. Lumped plasticity models are frequently used in structural analysis [14]–[16], since it is easier to implement [17]. When calibrated properly, it can capture degradation of strength and stiffness that is essential to collapse modeling. Also, it is easy to modify their properties in a sensitivity analysis to evaluate the uncertainties in material modeling. Since both have advantages, the choice of the numerical model should consider the available options and be carefully evaluated for a given structural system, since no single model is universally applicable [11].

In this regard, this paper presents a case study to compare Fiber and Lumped Plasticity Models using non-linear static and dynamic analyses, the latter being used to generate fragility functions. The differences in obtained results using both models are compared, and these differences can be used for decision-making in further works on seismic risk.

2 NUMERICAL MODELLING

Considering the several existing methods to simulate cyclic response on reinforced concrete buildings on a non-linear analysis, the aim of this paper is to compare the Fiber Model and the Lumped Plasticity Model. The Fiber Model consists of fiber beam-column elements, which considers plasticity distributed all along the element, and the Lumped Plasticity Model, with plastic-hinges, lumps the bond-slip and beam-column yielding on concentrated hinges [12]. The accurate modeling of inelastic behavior of beams and columns elements is essential for the collapse modeling of RC frame structures.

Salehi et al. [18] emphasize that all damage mechanisms (concrete and steel damage, bar buckling and bar slipping) on the concentrated plasticity elements are aggregated in the constitutive laws of the zero-length springs. So, they cannot predict

spread of damage over the member length, because the inelastic response is allowed in prescribed locations. However, distributed-plasticity models require only the constitutive laws of the materials, but they demand a considerable computational cost when considering force-based elements or considering a structure-level iterations, since the degrees of freedom increase. The considerations for both models are described in detail in the following sections. Information about material properties and damping in the analysis sections. Both models consider fixed bases, with no soil structure interaction. Also, neither one considers inelastic joint responses and column shear failures, with its columns being flexure critical.

2.1 Fiber Model

The Finite Element Model developed for the Fiber Model uses OpenSees [19] software and its library to create beams and columns elements. Figure 1 represents the model in a 2D frame.

Beams and columns are modeled using displacement-based beam-column elements with distributed plasticity and cross-sections divided into several fibers that separates confined and unconfined concrete and the longitudinal reinforcement steel. Beams are modeled with five finite elements in each bay (50 centimeters between each node), and columns are modeled with four elements between each story (75 centimeters between each node). Each finite element has three *Gauss-Lobatto* integration points. Three types of fiber sections are considered for the beams to account for the variation of longitudinal reinforcement in the mid-spam and near its two edges. For the columns, only one fiber section is considered, since the reinforcement ratio is the same for all stories. The cross section of beams and columns is discretized in 2 to 39 fibers, depending on direction and whether it is the confined concrete core or the concrete cover. The non-linear behavior of the materials is considered through all the element length.

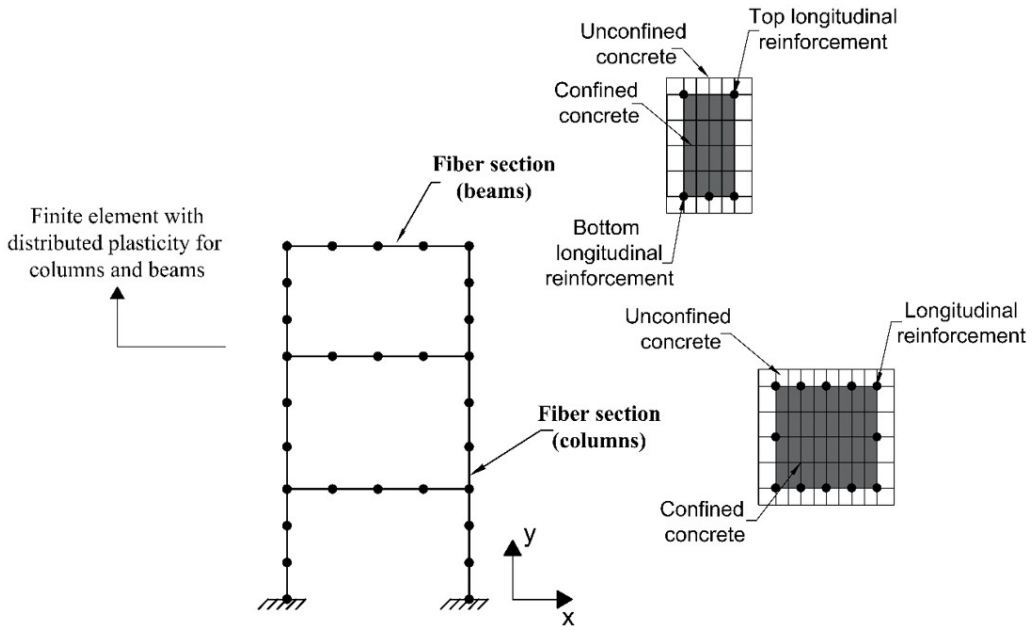

Figure 1. Generic representation of the Finite Element Model for the Fiber Model.

2.1.1 Constitutive law for concrete and steel

The constitutive law for confined and unconfined reinforced concrete used herein is the one proposed by Chang and Mander [20], which considers the increase in ductility and strength of the concrete due to the effect of the confinement provided by transverse reinforcement. The concrete cross-section of columns and beams consider a confined core and unconfined concrete cover. In the OpenSees library, the material is called *Concrete07*.

For steel, the constitutive model adopted is proposed by Guiffré-Menegetto-Pinto [21] (*Steel02* in OpenSees library) with isotropic strain hardening with 1% of hardening rate, as suggested by Carreño et al. [22]. Rebar fracture is not considered on this model. The modulus of elasticity of 210 GPa, and a yield strength of 500 MPa are adopted. This model has a soft transition between the elastic branch and steel yield. Figure 2 represents the constitutive law for concrete (left) and steel (right).

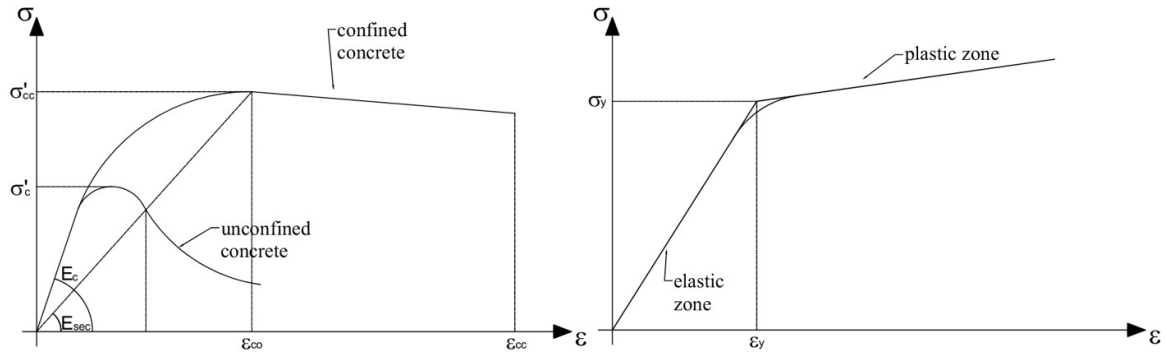

Figure 2. Constitutive laws for concrete (left) and steel (right).

2.2 Lumped Plasticity Model

The Finite Element Model developed for the lumped plasticity models uses OpenSees software and its own library to create beams and columns elements. Figure 3 represents the model in a 2D frame.

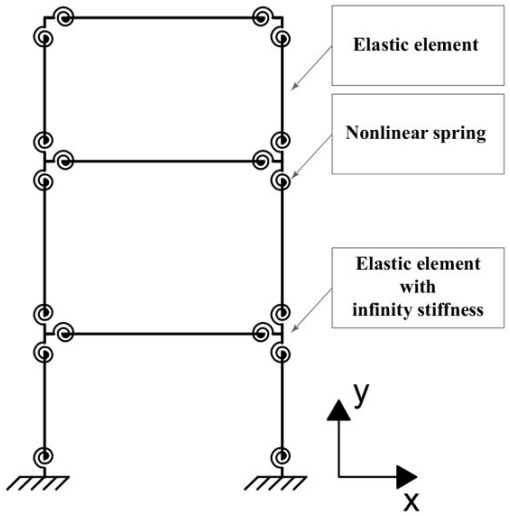

Figure 3. Representation of the Finite Element Model for the Lumped Plasticity Model.

For this, a non-linear spring model is used, developed by Ibarra et al. [23] and described with details in section 2.2.1. The material, named *uniaxialMaterial IMKPeakOriented* in OpenSees library, is applied to a zero-length element represented by the springs on Figure 3. Joints are represented by an elastic element with the length of the joint and infinite stiffness. The rest of the element is modelled also with *elasticBeamColumn* element with its area and Young's Modulus of the material. To account for the degradation of strength and stiffness associated with large deformations, suitable geometric transformations, and a leaning (P-Δ) column are used in the analysis. The effects of foundation flexibility have not been considered at this part of the model development.

2.2.1 Plastic Hinge Model

Lumped plasticity model is widely used to evaluate seismic vulnerability and has already been implemented on FEMA recommendations [11]. The lumped plasticity elements can capture the strain softening associated with rebar buckling and spalling phenomena, which are essential for simulating structural collapse in RC buildings [6]. For special reinforced concrete moment frames structures, the material used on OpenSees for the plastic hinge has been developed by Ibarra et al. [23], and the application of the material on reinforced concrete frames has been done by Haselton et al. [6]. It is chosen herein because it can capture the important modes of deterioration that precipitate sidesway collapse of RC frames [11].

The model is used to simulate the non-linear hysteretic response of reinforced concrete (RC) beams or columns under large deformations and is also developed to enable simulation of the non-linear dynamic response of RC frame buildings under earthquake ground motions. It consists of a monotonic backbone curve and hysteretic degradation rules to capture post-peak in-cycle softening which are associated with concrete crushing and reinforcing bar buckling at large cyclic deformations [6]. Figure 4 represents the monotonic curve by an idealized trilinear end moment (M) versus chord rotation (θ) response of an equivalent cantilever column.

The curve is defined considering five parameters: yield moment capacity M_y; initial elastic secant stiffness to yield point K_e; maximum moment capacity M_c; plastic chord rotation from yield to cap point $\theta_{cap,pl}$; post-capping plastic rotation capacity θ_{pc}. The flexural yield strength M_y generally is computed using a strain compatibility approach. It is assumed that sections remain plane and also an equivalent rectangular compressive stress distribution under ultimate loads with a concrete crushing strain of 0.003 [6]. The equations for the model's parameters are presented in the following sections. Interested readers are referred to Haselton et al. [24] and Haselton et al. [6] for more detailed information.

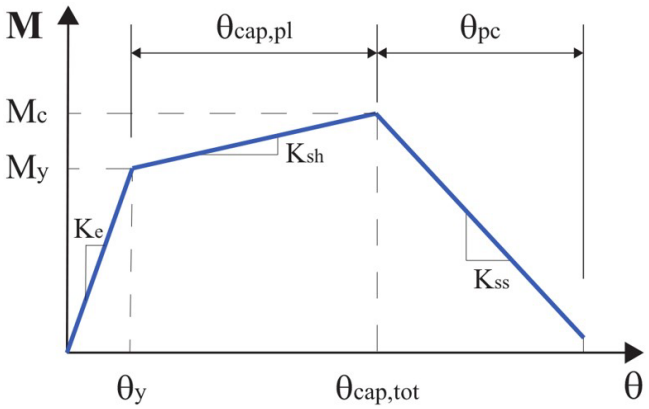

Figure 4. Idealized trilinear end moment versus chord rotation.

2.2.2 Effective Initial Stiffness (EI_y/EI_g and EI_{stf}/EI_g)

Two values of effective stiffness are defined: the secant stiffness to the yield point of the component (EI_y), represented by Equation 1; and the secant stiffness to 40% of the yield force of the component (EI_{stf}), represented by Equation 2. The values are expressed as a ratio of the gross cross-section stiffness (EI_g), and includes all modes of deformation: flexure, shear and bond-slip.

$$\frac{EI_y}{EI_g} = 0.30\left(0.1 + \frac{P}{A_g f_c'}\right)^{0.80}\left(\frac{L_s}{h}\right)^{0.72} \quad (1)$$

Where $0.2 \leq EI_y/EI_g \leq 0.6$.

$$\frac{EI_{stf}}{EI_g} = 0.77\left(0.1 + \frac{P}{A_g f_c'}\right)^{0.80}\left(\frac{L_s}{h}\right)^{0.43} \quad (2)$$

Where $0.35 \leq EI_{stf}/EI_g \leq 0.8$.

P corresponds to the axial load; A_g is the gross concrete area; f_c' is the compressive strength of unconfined concrete; L_s is the shear span, corresponding to the distance between column end and point of inflection; h is the cross-section height. EI_{stf} is expected to be approximately 1.7 times stiffer than the secant stiffness to yield EI_y in a typical column. The choice between which stiffness is adequate depends on the deformation levels expected in the analysis. EI_{stf} is generally used for analysis at low deformation demands below yield, and the yield stiffness EI_y is intended for higher

demands, where displacements are beyond yield and into the inelastic range. However, studies have shown that the value used for initial stiffness does not influence the response in a highly non-linear range and up to collapse [6].

2.2.3 Plastic rotation capacity ($\theta_{cap,pl}$)

Equation 3 is proposed to determine the rotation capacity (measured in radians) between yield and the peak moment resistance.

$$\theta_{cap,pl} = 0.12(1 + 0.55a_{sl})(0.16)^{\nu}(0.02 + 40\rho_{sh})^{0.43} \times (0.54)^{0.01c_{unit}f_c'}(0.66)^{0.1s_n}(2.27)^{10\rho} \quad (3)$$

Where: a_{sl} is an indicator variable (0 or 1) to signify possibility of longitudinal reinforcing bar slip beyond the column end; $a_{sl} = 1$ if slip is possible (defined by [25], [26]); ν is the axial load ratio, given by $\nu = P/A_g f_c'$; f_c' is the compressive strength of unconfined concrete, based on standard cylinder test; ρ_{sh} is the transversal reinforcement ratio; ρ is the longitudinal reinforcement ratio; c_{unit} is an unit conversion variable that equals 1 when f_c' and f_y are in MPa and 6.9 for ksi; s_n is the reinforcing bar slenderness ratio, given by $\frac{s}{d_b}$ (s corresponds to the spacing of transverse reinforcement measured along height of column and d_b is the longitudinal bar diameter). Since the experimental data used in the study are limited to columns with symmetrical arrangements of reinforcement, Equation 3 is only applied to columns following this configuration.

2.2.4 Post-capping rotation capacity (θ_{pc})

Equation 4 defines the post-capping rotation capacity.

$$\theta_{pc} = (0.76)(0.031)^{\nu}(0.02 + 40\rho_{sh})^{1.02} \leq 0.10 \quad (4)$$

The parameters that influence deformation capacity are axial load ratio, transverse steel ratio, reinforcing bar buckling coefficient, stirrup spacing, concrete strength and longitudinal steel ratio. On the calibration process there are only 15 tests suitable for θ_{pc}, because only in them the post-capping slope was clear [6].

2.2.5 Post-yield hardening stiffness

The prediction of hardening stiffness has the axial load ratio and concrete strength as statistically significant parameters. Despite that, the inclusion of both did not improve the regression analysis, and it is recommended a constant value that is represented in Equation (5) [6], [11], [24].

$$\frac{M_c}{M_y} = 1.13 \quad (5)$$

2.2.6 Cyclic energy dissipation capacity

Cyclic energy dissipation capacity can be quantified using two different expressions: $E_t = \gamma M_y \theta_y$ and $E_t = \lambda' M_y \theta_{cap,pl}$ that are defined by the parameters γ and λ'. The equations for each one of them are represented in (6) and (7), respectively.

$$\gamma = (170.7)(0.27)^{\nu}(0.10)^{s/d} \quad (6)$$

$$\lambda' = (30)(0.3)^{\nu} \quad (7)$$

Where: d is the depth of column cross-section. The use of λ' is more interesting because the energy dissipation capacity E_t is more highly correlated with the associated plastic rotation capacity. Despite that, OpenSees uses the value of γ for the material developed by Ibarra et al. [23], although it is referred as λ in the software library.

3 METHODOLOGY

Figure 5 summarizes the methodology used herein to compare both Finite Element Models on a static Pushover analysis and on a dynamic analysis. Further details are given below.

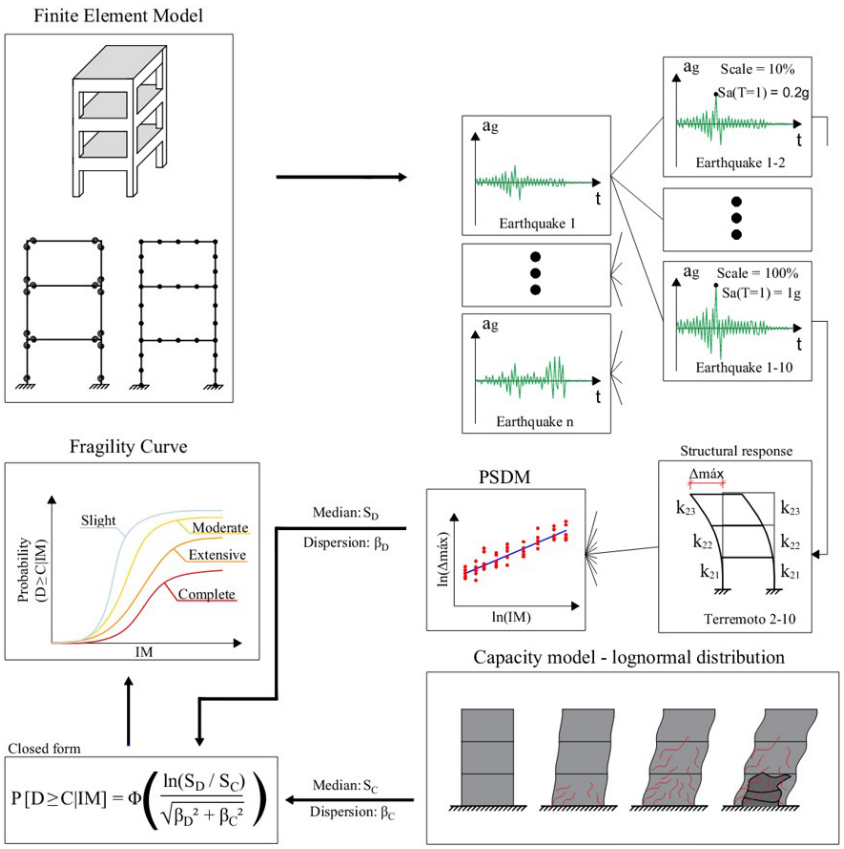

Figure 5. Summary of the methodology.

3.1 Non-linear static Pushover analysis

Pushover analysis (PA) consists of a non-linear static procedure carried out under constant gravitational loads and horizontal loads increasing monotonically. Its main goals are to verify the structural performance of buildings, by means of capacity curves (i.e., the building's base shear as a function of the building's roof displacement) and to estimate the expected plastic mechanism and the distribution of damage. It is an alternative, or a complement, to the common design-based procedures or linear-elastic analyses. Figure 6 represents the procedure, with the horizontal loads applied in a 2D frame.

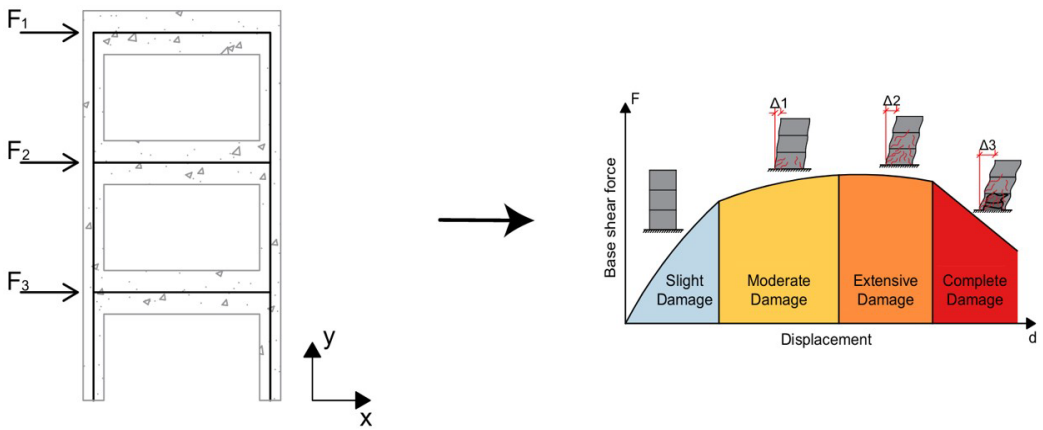

Figure 6. Representation of the Pushover Analysis and the Capacity Curve.

PA is described in several standards, each one of them accounting for different aspects of the definition of its procedures and the vertical distributions of the lateral loads that should be applied. The choice of vertical distributions of the lateral loads can influence the generated capacity curve (EUROCODE 8 [27] and FEMA-356 [28]). Since the aim of this work is to compare both finite element models and, therefore, comparison between load patterns is considered as out of the scope, we apply a load pattern proportional to the mass in each story. Once the load pattern is defined, the capacity curve is generated by relating the displacement of the top of the building with the total base shear observed during the analysis.

The structural capacity (C) is defined as the maximum response that a structure can withstand without reaching a limit state [29]. This article considers the qualitative and quantitative definitions of the Damage Limit States proposed in Hazus manual [30] for reinforced concrete moment resisting frames (C1), since it is a definition widely adopted in the literature, facilitating further comparison with other works. The qualitative definitions of the damage states, in terms of building performance, are presented in Table 1.

Table 1. Qualitative description of the Damage Limit States from Hazus [30].

Limit State	Qualitative Description
Slight Structural Damage (SSD)	Flexural or shear type hairline cracks in some beams and columns near joints or within joints.
Moderate Structural Damage (MSD)	Most beams and columns exhibit hairline cracks. In ductile frames some of the frame elements have reached yield capacity indicated by larger flexural cracks and some concrete spalling. Nonductile frames may exhibit larger shear cracks and spalling.
Extensive Structural Damage (ESD)	Some of the frame elements have reached their ultimate capacity indicated in ductile frames by large flexural cracks, spalled concrete and buckled main reinforcement; nonductile frame elements may have suffered shear failures or bond failures at reinforcement splices, or broken ties or buckled main reinforcement in columns which may result in partial collapse.
Complete Structural Damage (CSD)	Structure is collapsed or in imminent danger of collapse due to brittle failure of nonductile frame elements or loss of frame stability. Approximately 13% of the total area of C1 buildings with Complete damage is expected to be collapsed.

3.2 Dynamic Analysis and Development of Analytical Fragility Functions

Fragility functions describe, in a probabilistic way, the probability of an undesirable event, as a function of some measure of environmental excitation [31]. Specifically considering earthquake events, they evaluate the probability that the seismic demand (D) on a structural system exceeds its structural capacity (C), depending on an intensity measure. A common assumption is made that demand, capacity and the fragility functions follow a lognormal distribution [31], [32], and a closed-form solution for the fragility can be used [33], as shown in Equation 8.

$$P[D \geq C|IM] = \Phi\left[\frac{ln\left(\frac{S_D}{S_C}\right)}{\sqrt{\beta_D^2+\beta_C^2}}\right] \tag{8}$$

Where Φ corresponds to the standard normal cumulative distribution function (CDF), S_D and β_D are the median and dispersion of the seismic demand and S_C and β_C are the capacity median and logarithmic dispersion.

In this paper, the parameters of the demand are obtained combining the Incremental Dynamic Analysis procedure [34] and the Probabilistic Seismic Demand Model approach [35], as developed by Dhir et al. [36]. The structural model is subjected to a set of ground motion records scaled to different levels of IM; then the maximum structural demand is related to the intensity measure IM by means of a linear regression of both measures in the logarithmic space. Based on Cornell et al. [32], the relation between the median seismic demand (S_D) and the intensity measure is assumed to follow the power law represented in Equation 9, and it can be rewritten in the logarithmic space, as shown in Equation 10 [32]. The coefficients a and b are obtained straight from the linear regression, and the logarithmic dispersion β_D in calculated using Equation 11, where N is the number of simulations and d_i is the maximum demand on the RC frame.

$$S_D = a(IM)^b \tag{9}$$

$$ln\,(S_D) = ln\,a + b\,ln\,(IM) \tag{10}$$

$$\beta_D = \sqrt{\frac{\sum\left(ln\,(d_i) - ln\left(a\times(IM^2)\right)\right)^2}{N-2}} \tag{11}$$

In this paper, the intensity measure used is the Spectral Acceleration fixed at the period of 1 second ($S_a(T = 1)$). It is chosen because most of the studies on seismic hazard consider this period, as for example, in the recent study for seismic hazard in South America by Petersen et al. [37]. Also, it is easier to compare two proposed structural models, because their fundamental periods of vibration are different. The damage measure, used herein as the output of the corresponding non-linear dynamic analysis, is the inter-story drift ratio observed during the analysis among all stories. This choice is justified since this parameter is well related to structural damage and has also been adopted by several researchers and design standards [28], [38]–[40]. Values of drift higher than 10% were discarded from the PSDM evaluation, since it is the criteria adopted herein for defining global collapse and account for global dynamic instability [41], [42]. For each earthquake record, 100 simulations for the demand are conducted, since the signal is scaled in maximum acceleration values of $0.05g$ until $5g$ is reached.

Quantitative values for each Limit State, based on Table 1 and considering a low-rise structure (1 to 3 pavements) and a pre-code classification, which means that structures do not take seismic actions in consideration, are adopted considering values of median interstory drift capacity (Sc) of: 0.40% for SSD; 0.64% for MSD; 1.60% for ESD; 4.00% for CSD. Based on suggestions from Wen et al. [29], the same value for the capacity logarithmic dispersion of $\beta_C = 0.3$ is adopted for all Limit States. The consideration of the same value for β_c for all Limit States is a simplification, since higher Limit States have a greater uncertainty due to the complexity of structural behavior near the failure [43]. After the calculation of demand and capacity parameters, the fragility functions for each Limit State are calculated based on Equation 8.

3.3 Ground Motion Suite

To perform the Incremental Dynamic Analysis, a suite of ground motions is necessary, and they must reflect the reality of the events that might happen in the region of study. This is an important step in the PBEE methodology, and the recommendation is to use one of the following options: select and scale accelerograms from real events; generate an artificial suite, consistent with the earthquake hazard scenario of the region [44]. Nevertheless, recent studies show that still there is no consensus in the engineering community regarding which ground motions must be used to perform the time history analyses [45]. The appropriate choice depends on both the region of interest and the goals of the study.

Since the main goal of this study is to compare the two different Finite Element Models used in fragility analysis, ground motions from different parts of the world are adopted. Natural earthquake records are obtained from the Pacific Earthquake Engineering Research Center NGA-West2 database [46]. The parameters of distance to the fault and moment magnitude are used to limit the search and collect hazard consistent signals. Fault distance is limited to a minimum of 15 km and maximum of 100 km in order to avoid near-fault ground motions and to minimize regional attenuation effects, respectively [47], [48]. Moment magnitude is limited to a minimum of 4.0 and maximum of 6.5, since it is very unlikely that smaller events could cause severe damage [2] and the maximum is recommended to be about one order larger than the largest event in the region, as suggested by Budnitz et al. [49].

Figure 7 illustrates the 5%-damped spectrum and the geometric mean of the set used, represented by 10 earthquake signals. The curve in red indicates the mean spectrum for the considered group of signals, as defined in the sequel.

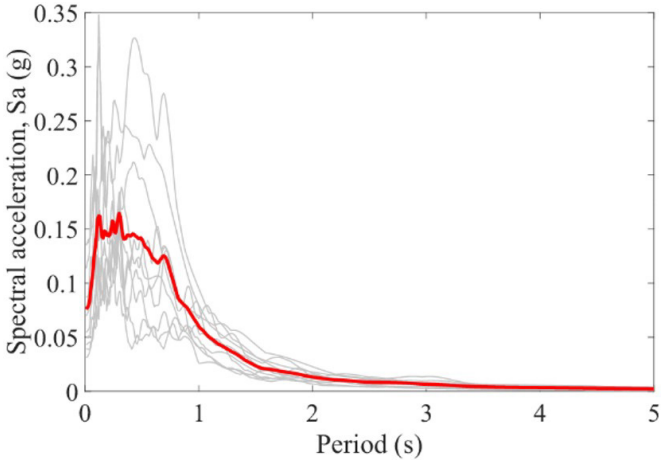

Figure 7. Mean spectral acceleration for the chosen signals.

4 RESULTS AND COMPARISON

4.1 Model Calibration

Experimental results available on the Pacific Earthquake Engineering Research Center (PEER) are used to check whether the numerical model developed is giving satisfactory results. Herein, the calibration process is described considering the results from experiment number 5 from Tanaka [50] for both Fiber and Lumped Plasticity models.

The experiment consists of a cyclic load applied in a column with 1.65 meters height and a rectangular cross-section which both width and depth have 55 centimeters. Column design considered 4 centimeters concrete cover, 12 longitudinal reinforcement bars of 20 millimeters diameter disposed in a symmetric way corresponding to a longitudinal reinforcement ratio of 1.25%. Transverse reinforcement is composed of two stirrups of 12 millimeters diameter with 11 centimeters spacing, representing a transverse reinforcement ratio of 1.7% and 4 shear legs. The yield stress of longitudinal and transverse reinforcement are 511MPa and 325MPa, respectively, and the ultimate stress are 675MPa for longitudinal and 429MPa for transverse bars. A representation of the column and the cross-section design detail is represented in Figure 8.

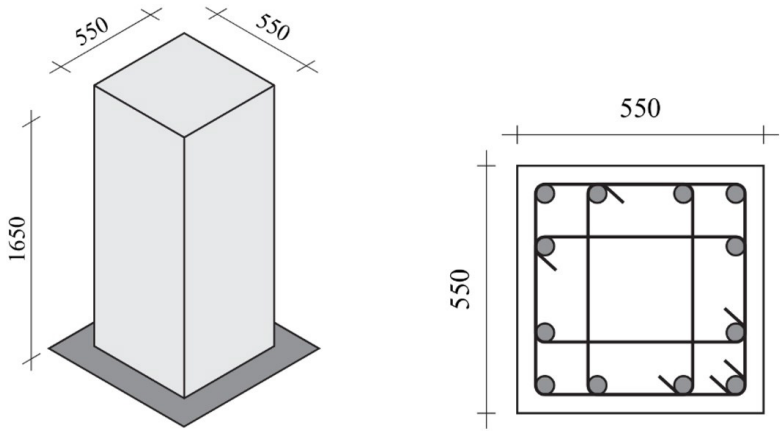

Figure 8. Representation of the column and its cross-section (in millimeters).

The numerical models for the Fiber Model and Lumped Plasticity Model are developed using OpenSees, based on the features of each model described in previous sections of this paper. Figure 9 shows the comparison between both models with the experimental results.

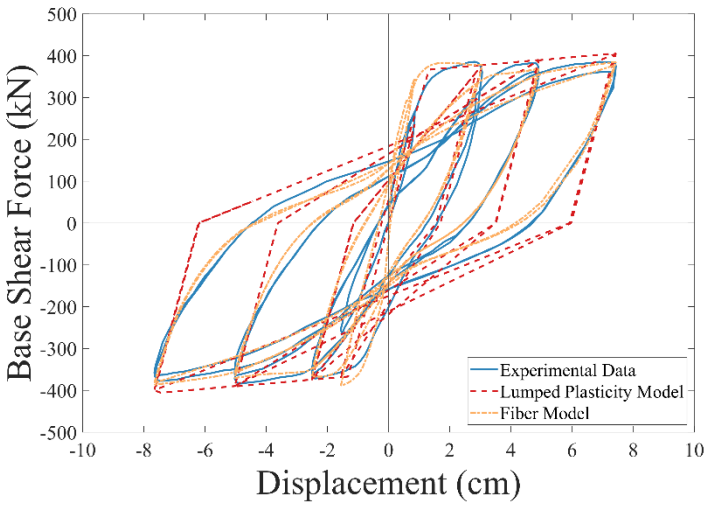

Figure 9. Displacement history applied at column top.

4.2 Static Analysis

This section shows a comparison between a Pushover analysis on the Fiber Model and the Lumped Plasticity Model. The methodology is applied on an example of a residential archetype building with a moment resisting frame structural system, designed using TQS software [51] according to ABNT NBR 6118 [52] with no seismic provisions. A two-bay model is considered as the minimum number of bays necessary to capture the behavior of interior and exterior columns and joints of structures, justifying the structural geometry chosen [53]. The structural elements have the same reinforcement in all floors. The 2D model considers a space frame system of the building, and Figure 10 illustrates the geometry of the building and the cross-sections of beams and columns.

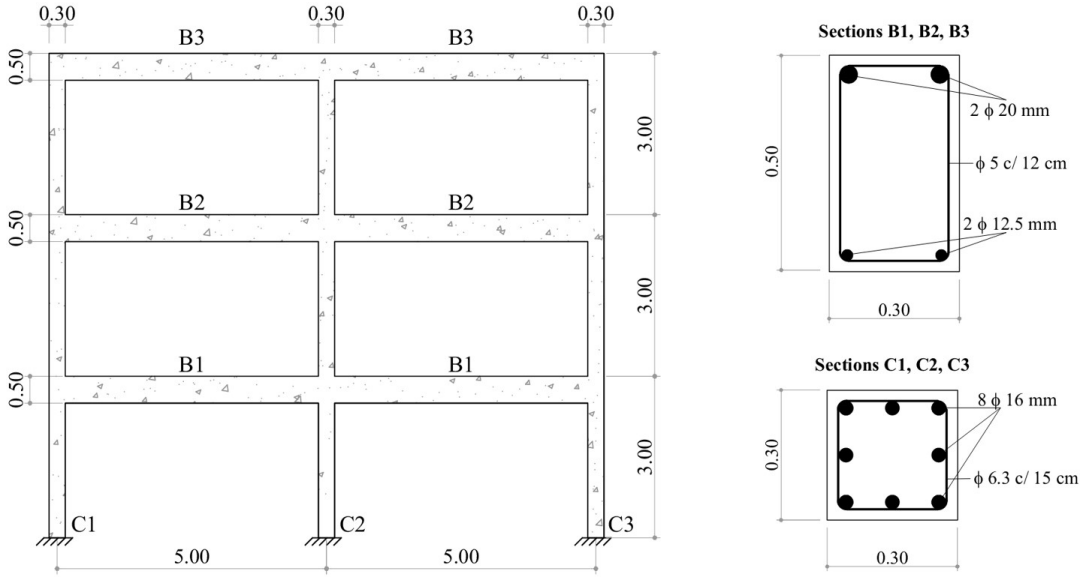

Figure 10. Representation of the 2D model simulated (units in meters).

The design considers a compressive strength of concrete of 23 MPa with Young's Modulus of $E = 22540MPa$, steel CA- 50 with Young's Modulus of $E = 210000MPa$, and the concrete cover is 2.50 centimeters. For the Fiber Model, internal nodes are placed on columns and beams with a 50 centimeters distance. Expected gravity loads are applied in the structure as uniformly distributed loads on the beams and they are used to define seismic masses on the model. These loads include 1.05 the dead load and 0.5kN/m^2 for live load, as adopted by Liel [53], which consists of 25% of the 2.0kN/m^2 maximum live load for residential buildings established in ABNT NBR 6120 [54]. P-Delta effects are considered in the columns.

Fundamental periods for both models are determined using OpenSees software. For the Lumped Plasticity Model, the fundamental horizontal period is 0.77 seconds, whereas the Fiber Model has a fundamental period of 0.34 seconds. Fundamental periods of the Lumped Plasticity Model tend to be larger than the Fiber Model. A reason for this leans on the fact that the model period of the LPM represents a secant stiffness (EI_{stf} in this analysis) rather than initial stiffness, and accounts for both flexural and bond-slip deformations in reinforced concrete elements [53]. The results of the Static Pushover analysis and the Capacity Curve for both models are represented on Figure 11.

The results show that both models reach approximately the same maximum base shear force value (280.9kN for the Lumped Plasticity Model and 272.4kN for the Fiber Model). Both models reach a plastic displacement between 5 and 10 centimeters. The ultimate displacement cannot be compared, since the constitutive law of steel does not have a descending branch, being necessary to define arbitrarily the rupture. This paper only considers softening for concrete, and common issues reported in the literature about the strain singularities during material softening [18] are not an object of study herein. The curve of the Lumped Plasticity Model agrees with the idealized monotonic curve for the model, represented in Figure 4. The differences in the stiffness of both models are expected, due to the use of a secant stiffness adopted in the lumped plasticity, whereas the fiber model's stiffness depends on the material's constitutive law, an issue also evidenced by the different periods of vibration obtained with the two models.

Slight and Moderate Limit State is reached at similar displacement for both models, with values of displacement of 2.5 centimeters for the Lumped Plasticity Model and 2 centimeters for the Fiber Model for Slight Limit State and 4 centimeters

for the Lumped Plasticity Model and 3 centimeters for the Fiber Model for the Moderate Limit State. For the other Limit States, the displacements have a higher difference, being 7 and 14,5 centimeters on the Fiber Model against 9 and 20 centimeters on the Lumped Plasticity Model for Extensive and Complete Limit States, respectively. Since the quantitative definitions of the Damage Limit States proposed in Hazus manual [30] considers the median interstory drift capacity (S_c) from the first floor of the building, the difference of the displacements observed in the Capacity Curve comes from the relative displacement between second - first floor and third - second floor. This means that, considering the Complete Limit State, the interstory drift capacity from the first floor of the building of 4% is reached on the Fiber Model when the top displacement of the building is 14,5 centimeters, whereas this value is reached on the Lumped Plasticity Model when the top displacement of the building is 20 centimeters. It indicates that the relative displacement between third and first floor is higher for the Lumped Plasticity Model when compared to the Fiber Model. Table 2 shows the shear forces on each limit state boundary for the two models, and the variation of the values.

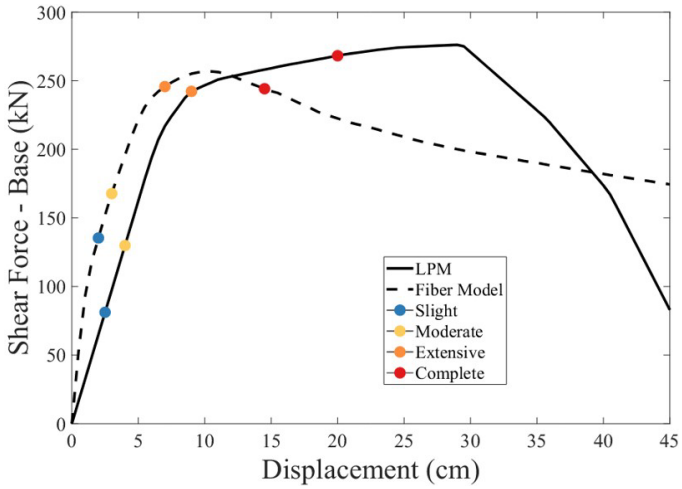

Figure 11. Comparison of Pushover results and Capacity Curve for Fiber and Lumped Plasticity Models.

The smallest variations found between the two models are the ones corresponding to Extensive and Complete Limit States. This behavior is expected, since the Lumped Plasticity Model has essential tools to capture the structural collapse in RC buildings. The exceedance of the Extensive state on the Lumped Plasticity Model occurs on the upward branch of the curve, which represents a more yield behavior on the Lumped Plasticity Model than in the Fiber Model.

Table 2. Shear Force values and variation for each Limit State.

Limit States / Shear Force Value (kN)	Lumped Plasticity Model	Fiber Model	Relative difference (%)
Slight	81.18	135.35	66.73
Moderate	129.89	167.73	29.13
Extensive	242.24	245.73	1.44
Complete	268.22	244.19	9.84

In order to evaluate how the structure behaves during the steps of the static analysis, the element deformation of the third degree of freedom for beams and columns are assessed in the four Damage Limit States used herein. The maximum value of deformation in each Limit State is found, and it represents the boundary between each Limit States. Colors blue, yellow, orange and red are used to indicate maximum deformation on Slight, Moderate, Extensive and Complete States, respectively. The increment of the curvature at the critical section of columns and beams can be seen in Figure 12 for the Lumped Plasticity Model and in Figure 13 for the Fiber Model.

From Figure 12, it can be confirmed the conclusion from the capacity curve that the difference in displacements observed in Extensive and Complete Limit States for both models come from the relative displacement between second and first floor and third and second floor. The Fiber Model does not present significant deformation on columns of third floor in any of the Limit States considered, while these columns in Lumped Plasticity Model present significant deformations since Extensive Limit State.

The deformations determined in the LPM have lower values than those obtained in the Fiber Model, which occurs due to the descending branch of the Moment-Curvature curve during the post-capping plastic rotation capacity. The constitutive law applied to the longitudinal reinforcement in the Fiber Model does not have a descending branch, then concentrating the damage at the critical cross-sections, reducing the damage distribution to other sections. Both models show that deformation increases more quickly on columns connecting ground floor to first floor, indicating strong beam - weak column behavior on the building. Figure 14 illustrate the Moment-Curvature curves for Lumped Plasticity Model and for the Fiber Model, considering the cross-sections located on the base of the columns C1, C2 and C3 connected to the ground. Since the EI relation for both moments is known, curvature on this case is obtained considering the equation: $d^2v/dx^2 = -M(x)/EI$ on each step of the analysis. It is important to emphasize that EI relation is kept constant during every step.

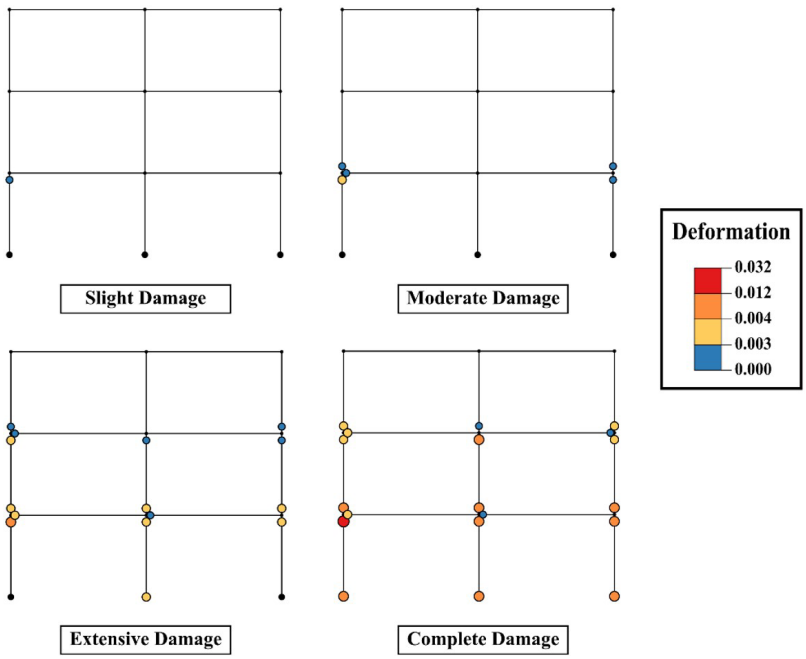

Figure 12. Evaluation of the element´s deformation for each Damage Limit State for the Lumped Plasticity Model.

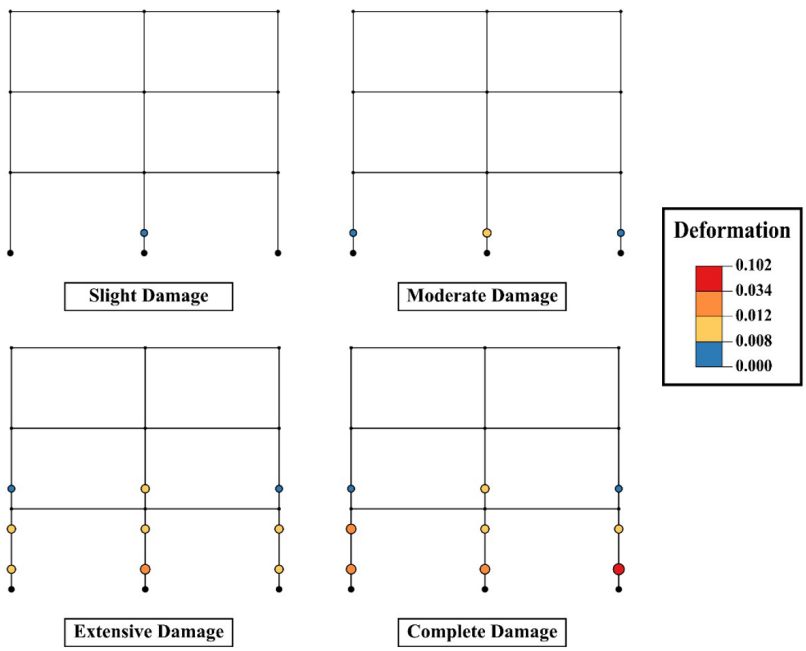

Figure 13. Evaluation of the element´s deformation for each Damage Limit State for the Fiber Model.

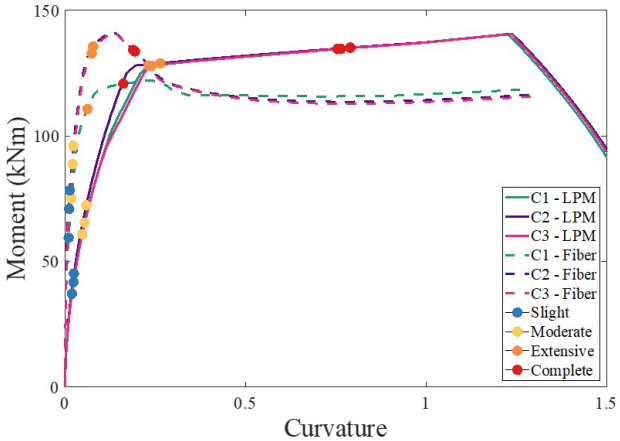

Figure 14. Moment-Curvature curves for Lumped Plasticity Model and Fiber Model for base columns of the first floor.

Table 3 illustrates the value of curvature for each column for all the Limit States considered, calculated for both models.

Table 3. Limit Curvature for each Limit State.

Damage Limit State	Lumped Plasticity Model			Fiber Model		
	C1	C2	C3	C1	C2	C3
Slight	0.019	0.024	0.023	0.009	0.013	0.011
Moderate	0.048	0.059	0.054	0.048	0.059	0.054
Extensive	0.231	0.264	0.241	0.063	0.078	0.074
Complete	0.754	0.790	0.764	0.161	0.194	0.189

Considering the differences described herein, the comparison of the static analyses indicates that both models can capture the damage level of the critical cross-sections. Furthermore, it is noticeable the prevalence of damage on the columns, instead of on beams. This is consistent with the damage pattern expected in reinforced concrete frames not designed according to modern seismic provisions such as the one herein. Both models can capture the formation of a column-sway mechanism in the building's first story, which is also undesirable from the structural safety point of view, since it tends to reduce the building's overall ductility. This should bring concern about the expected structural performance of non-seismic buildings designed according to the ABNT NBR 6118 [52], and outlines the need for more studies in this line.

4.3 Dynamic Analysis and Fragility Curves

Besides the static analysis, a comparison of the two models in dynamic analyses is performed considering the earthquake accelerograms. These analyses consider the steps described in the methodology of this paper, including Incremental Dynamic Analysis (IDA), probabilistic seismic design models (PSDM) and calculation of the fragility curves. Rayleigh damping corresponding to $\xi = 5\%$ of critical damping is adopted using the first and third frequencies. Figure 15 represents the results for the probabilistic seismic demand model (PSDM) for the Lumped Plasticity Model (left) and for the Fiber Model (right).

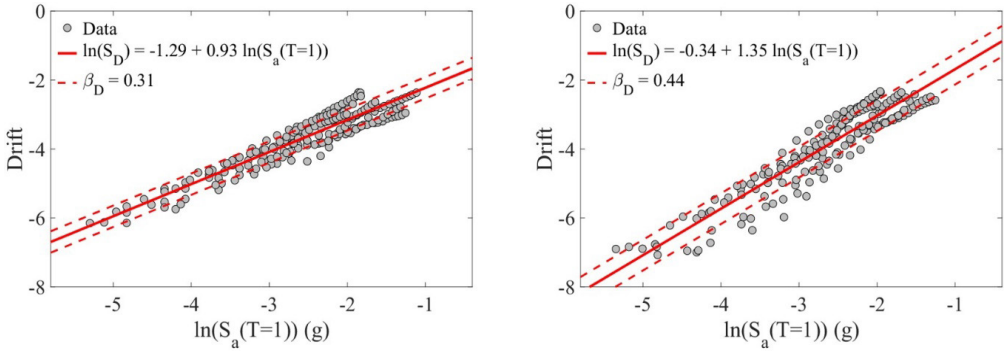

Figure 15. PSDM results for the Lumped Plasticity Model (left) and Fiber Model (right).

A residual analysis (Drift from LPM models – Drift from Fiber models) in logarithmic space is realized to show in a better way the difference between drifts from the Lumped Plasticity Model and Fiber Model, as represented on Figure 16. Note that there is a tendency for the drift obtained using LPM to be higher after a certain range of Sa(T=1) values, which agrees with the previous results (see Figures 11 and 14).

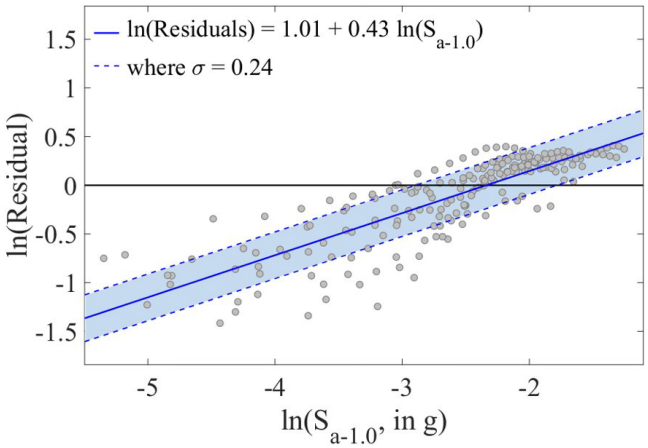

Figure 16. Residual analysis with the PSDM results.

The Lumped Plasticity model has a lower dispersion value than the Fiber Model. The dispersion is an important parameter to be compared, since it is only related to the Finite Element Model. The accelerograms used in the analyses with both models are the same. The results of the fragility curves are represented in Figure 17.

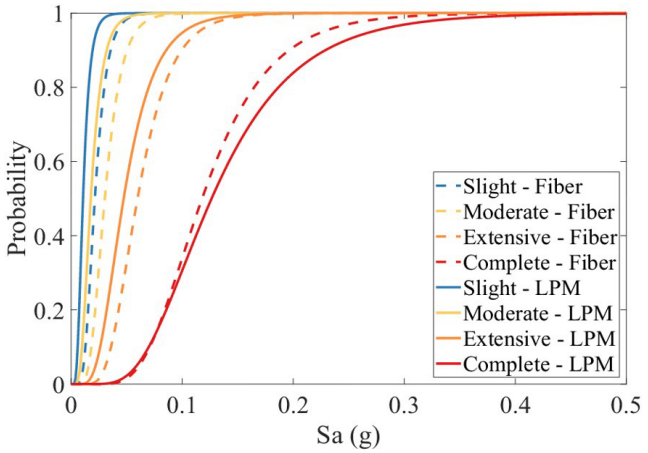

Figure 17. Comparison of the fragility curves for the Lumped Plasticity Model and Fiber Model.

Table 4 represents the median and logarithmic dispersion values for the represented fragility curves.

Table 4. Median and logarithmic dispersion for the Fragility Curves.

Damage Limit State	Lumped Plasticity Model		Fiber Model	
	Median	Dispersion	Median	Dispersion
Slight	0.0107	0.4629	0.0214	0.3977
Moderate	0.0177	0.4629	0.0303	0.3977
Extensive	0.0473	0.4629	0.0598	0.3977
Complete	0.1265	0.4629	0.1179	0.3977

The results indicate that the fragility curves for the Slight and Moderate Damage Limit States have a significant difference between the two models. The Lumped Plasticity Model (LPM) leads to a probability of exceedance of 100% with a median value of 0.0107g and 0.0177g for Slight and Moderate Limit State, respectively, whereas the Fiber Model has medians of 0.0214g and 0.0303g for Slight and Moderate Limit States, respectively. For Slight, Moderate and Extensive limit states, the probability of exceedance of the LPM is higher than in the Fiber Model. Considering an acceleration $S_a = 0.08g$ and the Extensive Limit State, Fiber Model has a probability of exceedance of 76.8%, whereas the Lumped Plasticity Model presents a probability of 87.2%.

However, for the Complete Damage, the curves behave in a different way. Considering a spectral acceleration value of $S_a = 0.2g$, the probability of exceedance of Complete Damage for the Fiber model corresponds to 90.8%, while the Lumped Plasticity presents a probability of 83.88%. This shows the inverse behavior from the other Damage Limit States, since the Fiber Model has a higher probability of exceedance of 100% before the Lumped Plasticity, being more conservative.

This observed behavior of the fragility curves also agrees with the results from the Static Analysis on the previous section. The Slight, Moderate and Extensive Limit States are reached by the Lumped Plasticity Model with a lower values of applied shear base force when compared to the Fiber Model, which means that this Limit States are easier to reach on the LPM Model. On the other hand, it is necessary a higher base shear force on the Lumped Plasticity Model than in the Fiber Model to reach the Complete Limit State, which may explain why the Fiber Model has a higher probability of exceedance of 100% before the LPM only on this Limit State.

5 CONCLUSIONS

This paper presents an attempt to understand the differences in the structural response of a 2D frame, modelled considering Fiber Model, which considers distributed plasticity along the structural element, and Lumped Plasticity Model, that considers plasticity concentrated in plastic hinges on the element.

Based on the results for the static analysis, the comparison showed that both models represent the maximum shear force on the base of the structure in a satisfactory way. The values for the force in both curves are approximately the same, with a relative error of 3%. There is a difference in the stiffness of the models, because the LPM uses a secant stiffness, which also influences in the period of vibration of the models. The Pushover curve of the Fiber Model has a limitation to represent structural collapse, which must be arbitrarily stipulated. For this reason, the ultimate displacements cannot be compared. The curve of shear forces and displacements of the Lumped Plasticity model agrees with the monotonic curve idealized for its representation. Also, the curvatures of the structure in both models are in agreement with their Moment x Curvature curves.

For the dynamic analysis, the two models have a better correspondence in their answers for the Damage Limit States Extensive and Complete Damage. The internal nodes discretization in the Fiber Model makes it able to capture in a more specific way the behavior of the structure at the beginning of the analyses. The use of the Lumped Plasticity Model is suitable when focusing the analysis on structural collapse, as proposed in Haselton et al. [24], where both have a similar answer.

The results from static and dynamic analysis don't give enough reasons to say which of the models is better than the other. The decision on which one to use may be based on the main goals of the research, and the technological resources available, since the analysis with the Lumped Plasticity Model is faster than the Fiber Model, demanding less computational effort. To put in numbers, the Pushover analysis with the LPM took 15,67 seconds to be completed, whereas the Fiber model took 30,19 seconds, both being done on the same computer. It means that in these analyses the LPM was 1,92 times faster than the Fiber Model, a significant difference depending on the number of analyses to be developed.

ACKNOWLEDGEMENTS

This study was financed in part by the São Paulo Research Foundation (FAPESP) - Finance Codes 2018/23304-9 and 2019/18368-0; the Coordenação de Aperfeiçoamento de Pessoal de Nível Superior - Brasil (CAPES) - Finance Code 001; the National Council for Scientific and Technological Development - CNPq, Brazil – Finance Code # 308040/2021-0. The authors would like to thank the company TQS Informática Ltda. for providing the academic version of the software CAD/TQS V21 used to design the building in this paper.

REFERENCES

[1] M. Assumpção, M. Pirchiner, J. C. Dourado, and L. V. Barros, "Terremotos no Brasil: preparando-se para eventos raros," *Soc. Bras. Geofísica, Bol. SBGf*, no. 96, pp. 25–29, 2016.

[2] C. I. Nievas, J. J. Bommer, H. Crowley, J. Van Elk, M. Ntinalexis, and M. Sangirardi, "A database of damaging small-to-medium magnitude earthquakes," *J. Seismol.*, vol. 24, pp. 263–292, 2020, http://dx.doi.org/10.1007/s10950-019-09897-0.

[3] M. Takeya, J. M. Ferreira, R. G. Pearce, M. Assumpção, J. M. Costa, and C. M. Sophia, "The 1986–1988 intraplate earthquake sequence near João Câmara, northeast Brazil—evolution of seismicity," *Tectonophysics*, vol. 167, no. 2-4, pp. 117–131, Oct 1989, http://dx.doi.org/10.1016/0040-1951(89)90062-0.

[4] C. Chimpliganond, M. Assumpção, M. Von Huelsen, and G. S. França, "The intracratonic Caraíbas–Itacarambi earthquake of December 09, 2007 (4.9 mb), Minas Gerais State, Brazil," *Tectonophysics*, vol. 480, no. 1-4, pp. 48–56, Jan 2010, http://dx.doi.org/10.1016/J.TECTO.2009.09.016.

[5] L. Reiter, *Earthquake Hazard Analysis: Issues and Insights*. New York: Columbia University Press, 1991. vol. 22, no. 3.

[6] C. B. Haselton, A. B. Liel, S. C. Taylor-Lange, and G. G. Deierlein, "Calibration of model to simulate response of reinforced concrete beam-columns to collapse," *ACI Struct. J.*, vol. 113, no. 6, pp. 1141–1152, Nov. 2016, http://dx.doi.org/10.14359/51689245.

[7] H. Krawinkler, "Challenges and progress in performance-based earthquake engineering," in *International Seminar on Seismic Engineering for Tomorrow--In Honor of Professor Hiroshi Akiyama*, 1999, vol. 26.

[8] Federal Emergency Management Agency, *Seismic Performance Assessment of Buildings - Methodology*, FEMA P-58-1, 2012.

[9] J. Moehle and G. G. Deierlein, *A Framework Methodology for Performance-based Earthquake Engineering*. 2004. (accessed Sep. 10, 2021). [Online]. Available: https://www.researchgate.net/publication/228706335

[10] G. H. Siqueira, A. S. Sanda, P. Paultre, and J. E. Padgett, "Fragility curves for isolated bridges in eastern Canada using experimental results," *Eng. Struct.*, vol. 74, pp. 311–324, Sep 2014, http://dx.doi.org/10.1016/J.ENGSTRUCT.2014.04.053.

[11] Federal Emergency Management Agency, *FEMA P695 - Quantification of Building Seismic Performance Factors*. Redwood, USA: Applied Technology Council, 2009.

[12] C. Haselton and G. G. Deierlein, "Assessing seismic collapse safety of modern reinforced concrete moment-frame buildings," *Pac. Earthq. Eng. Res. Cent.*, vol. 8, no. Feb., pp. 295, 2008.

[13] E. Bruschi, P. M. Calvi, and V. Quaglini, "Concentrated plasticity modelling of RC frames in time-history analyses," *Eng. Struct.*, vol. 243, pp. 112716, Sept. 2021, http://dx.doi.org/10.1016/j.engstruct.2021.112716.

[14] P. B. Murray, A. B. Liel, and K. J. Elwood, "A framework for assessing impaired seismic performance as a trigger for repair," *Earthquake Eng. Struct. Dynam.*, vol. 51, no. 2, pp. 438–456, Feb. 2022, http://dx.doi.org/10.1002/eqe.3573.

[15] C. A. Goulet et al., "Evaluation of the seismic performance of a code-conforming reinforced-concrete frame building - From seismic hazard to collapse safety and economic losses," *Earthquake Eng. Struct. Dynam.*, vol. 36, no. 13, pp. 1973–1997, Oct. 2007, http://dx.doi.org/10.1002/EQE.694.

[16] E. A. Opabola, K. J. Elwood, and A. B. Liel, "Evaluation of seismic performance of as-built and retrofitted reinforced concrete frame structures with LAP splice deficiencies," *Earthquake Eng. Struct. Dynam.*, vol. 50, no. 12, pp. 3138–3159, Oct. 2021, http://dx.doi.org/10.1002/EQE.3503.

[17] R.-Y. Wu and C. P. Pantelides, "Concentrated and distributed plasticity models for seismic repair of damaged RC bridge columns," *J. Compos. Constr.*, vol. 22, no. 5, pp. 04018044, Aug. 2018, http://dx.doi.org/10.1061/(asce)cc.1943-5614.0000879.

[18] M. Salehi, P. Sideris, and A. B. Liel, "Assessing damage and collapse capacity of reinforced concrete structures using the gradient inelastic beam element formulation," *Eng. Struct.*, vol. 225, Dec. 2020, http://dx.doi.org/10.1016/J.ENGSTRUCT.2020.111290.

[19] F. McKenna, G. L. Fenves, and M. H. Scott, "OpenSees: open system for earthquake engineering simulation," *Pacific Earthq. Eng. Res. Center, Univ. Calif.*, 2006. (accessed Sep. 10, 2021). [Online]. Available: http://opensees.berkeley.edu

[20] G. A. Chang and J. B. Mander, *Seismic Energy Based Fatigue Damage Analysis of Bridge Columns: Part 1 - Evaluation of Seismic Capacity.* Buffalo, NY: National Center for Earthquake Engineering Research, 1994.

[21] F. C. Filippou, V. V. Bertero, and E. P. Popov, *Effects of Bond Deterioration on Hysteretic Behavior of Reinforced Concrete Joints*. California: Earthquake Engineering Research Center, University of California, 1983.

[22] R. Carreño, K. H. Lotfizadeh, J. P. Conte, and J. I. Restrepo, "Material model parameters for the giuffrè-menegotto-pinto uniaxial steel stress-strain model," *J. Struct. Eng.*, vol. 146, no. 2, pp. 04019205, Dec. 2019, http://dx.doi.org/10.1061/(ASCE)ST.1943-541X.0002505.

[23] L. F. Ibarra, R. A. Medina, and H. Krawinkler, "Hysteretic models that incorporate strength and stiffness deterioration," *Earthquake Eng. Struct. Dynam.*, vol. 34, no. 12, pp. 1489–1511, Oct. 2005, http://dx.doi.org/10.1002/EQE.495.

[24] C. Haselton, A. Liel, S. Lange, and G. Deierlein, "Beam-column element model calibrated for predicting flexural response leading to global collapse of RC frame buildings," *Pac. Earthq. Eng. Res. Cent.*, vol. 3, no. May, pp. 152, 2008.

[25] M. N. Fardis and D. E. Biskinis, Deformation capacity of RC members, as controlled by flexure or shear, in *Otani Symposium*, 2003, vol. 511530.

[26] T. B. Panagiotakos and M. N. Fardis, "Deformations of reinforced concrete members at yielding and ultimate," *Struct. J.*, vol. 98, no. 2, pp. 135–148, 2001.

[27] European Standard, *Eurocode 8: Design of structures for earthquake resistance - Part 1 : General Rules, Seismic Actions and Rules for Buildings*, EN 1998-1, 2004.

[28] Federal Emergency Management Agency, F*EMA 356 - Prestandard and Commentary for the Seismic Rehabilitation of Buildings*. Washington, DC, USA: American Society of Civil Engineers, 2000.

[29] Y. K. Wen, B. R. Ellingwood, and J. M. Bracci, *Vulnerability Function Framework for Consequence-based Engineering*, 2004 (accessed Sep. 10, 2021). [Online]. Available: https://www.ideals.illinois.edu/handle/2142/9177

[30] Earthquake Loss Estimation Methodology, *Hazus - MH 2.1 Advanced Engineering Building Module (AEBM) Technical and User's Manual*. Washington, DC, USA: Federal Emergency Management Agency, 2015.

[31] K. Porter, *A Beginner's Guide to Fragility, Vulnerability, and Risk*. Boulder, USA: Univ. Colorado Boulder, 2021. Accessed Sep. 10, 2021. [Online]. Available: http://spot.colorado.edu/~porterka/Porter-beginners- guide.pdf

[32] C. A. Cornell, F. Jalayer, R. O. Hamburger, and D. A. Foutch, "Probabilistic basis for 2000 SAC Federal emergency management agency steel moment frame guidelines," *J. Struct. Eng.*, vol. 128, no. 4, pp. 526–533, Apr. 2002, http://dx.doi.org/10.1061/(ASCE)0733-9445(2002)128:4(526).

[33] E. Choi and J.-C. Jeon, "Seismic fragility of typical bridges in moderate seismic zone," *KSCE J. Civ. Eng.*, vol. 7, no. 1, pp. 41–51, 2003.

[34] D. Vamvatsikos and C. A. Cornell, "Incremental dynamic analysis," *Earthquake Eng. Struct. Dynam.*, vol. 31, no. 3, pp. 491–514, Mar. 2002, http://dx.doi.org/10.1002/EQE.141.

[35] J. E. Padgett, *Seismic Vulnerability Assessment of Retrofitted Bridges Using Probabilistic Methods*, Atlanta, GA, USA: Georgia Institute of Technology, 2007.

[36] P. K. Dhir, N. P. Zade, A. Basu, R. Davis, and P. Sarkar, "Implications of Importance factor on seismic design from 2000 SAC-FEMA perspective," *ASCE ASME J. Risk Uncertain. Eng. Syst. A Civ. Eng.*, vol. 6, no. 2, pp. 04020016, 2020, http://dx.doi.org/10.1061/ajrua6.0001048.

[37] M. D. Petersen et al., "Seismic hazard, risk, and design for South America," *Bull. Seismol. Soc. Am.*, vol. 108, no. 2, pp. 781–800, Apr 2018, http://dx.doi.org/10.1785/0120170002.

[38] A. Whittaker, R. O. Hamburger, C. Comartin, M. Mahoney, R. Bachman, and C. Rojahn, Performance-based engineering of buildings and infrastructure for extreme loadings, in *AISC-SINY Symposium on Resisting Blast and Progressive Collapse*, New York, American Institute of Steel Construction, 2003.

[39] S. K. Ramamoorthy, P. Gardoni, and J. M. Bracci, "Probabilistic demand models and fragility curves for reinforced concrete frames," *J. Struct. Eng.*, vol. 132, no. 10, pp. 1563–1572, Oct. 2006, http://dx.doi.org/10.1061/(ASCE)0733-9445(2006)132:10(1563).

[40] S. K. Ramamoorthy, P. Gardoni, and J. M. Bracci, "Seismic fragility and confidence bounds for gravity load designed reinforced concrete frames of varying height," *J. Struct. Eng.*, vol. 134, no. 4, pp. 639–650, Apr. 2008, http://dx.doi.org/10.1061/(ASCE)0733-9445(2008)134:4(639).

[41] F. Jalayer, H. Ebrahimian, A. Miano, G. Manfredi, and H. Sezen, "Analytical fragility assessment using unscaled ground motion records," *Earthquake Eng. Struct. Dynam.*, vol. 46, no. 15, pp. 2639–2663, Dec. 2017, http://dx.doi.org/10.1002/EQE.2922.

[42] B. W. Baird, A. B. Liel, M. Eeri, and R. E. Chase, "Magnitude thresholds and spatial footprints of damage from induced earthquakes," *Earthq. Spectra*, vol. 36, no. 4, pp. 1995–2018, 2020, http://dx.doi.org/10.1177/8755293020935138.

[43] D. H. Tavares, J. E. Padgett, and P. Paultre, "Fragility curves of typical as-built highway bridges in eastern Canada," *Eng. Struct.*, vol. 40, pp. 107–118, Jul. 2012, http://dx.doi.org/10.1016/J.ENGSTRUCT.2012.02.019.

[44] J. J. Bommer, S. G. Scott, and S. K. Sarma, "Hazard-consistent earthquake scenarios," *Soil. Dyn. Earthquake Eng.*, vol. 19, no. 4, pp. 219–231, Jun. 2000, http://dx.doi.org/10.1016/S0267-7261(00)00012-9.

[45] N. R. Manzo and M. F. Vassiliou, "Displacement-based analysis and design of rocking structures," *Earthquake Eng. Struct. Dynam.*, vol. 48, no. 14, pp. 1613–1629, Nov. 2019, http://dx.doi.org/10.1002/EQE.3217.

[46] Open Berkeley, "PEER strong ground motion databases." Pacific Earthquake Engineering Research Center. Available: https://peer.berkeley.edu/peer-strong-ground-motion-databases (accessed Sep. 10, 2021).

[47] R. A. Medina and H. Krawinkler, *Seismic Demands for Nondeteriorating Frame Structures and their Dependence on Ground Motions*, 2003 (accessed Sep. 10, 2021). [Online]. Available: http://blume.stanford.edu

[48] J. J. Bommer, P. J. Stafford, and J. E. Alarcón, "Empirical equations for the prediction of the significant, bracketed, and uniform duration of earthquake ground motionempirical equations for the prediction of the duration of earthquake ground motion," *Bull. Seismol. Soc. Am.*, vol. 99, no. 6, pp. 3217–3233, Dec. 2009, http://dx.doi.org/10.1785/0120080298.

[49] R. J. Budnitz, G. Apostolakis, and D. M. Boore, *Recommendations for Probabilistic Seismic Hazard Analysis: Guidance on Uncertainty and Use of Experts*. USA: U.S. Nuclear Regulatory Commission, 1997, http://dx.doi.org/10.2172/479072.

[50] H. Tanaka, *Effect of Lateral Confining Reinforcement on the Ductile Behaviour of Reinforced Concrete Columns*, Christchurch, New Zealand: University of Canterbury, 1990.

[51] TQS, "CAD/TQS Plena." TQS, 2019. Available: http://www.tqs.com.br/conheca-os-sistemas-cadtqs/analise-estrutural/95-modelo-tqs (accessed Sep. 10, 2021).

[52] Associação Brasileira de Normas Técnicas, *Projeto de Estruturas de Concreto — Procedimento*, NBR 6118, 2014.

[53] A. B. Liel, *Assessing the Collapse Risk of California's Existing Reinforced Concrete Frame Structures: Metrics for Seismic Safety Decisions*. Stanford, USA: Stanford University, 2008.

[54] Associação Brasileira de Normas Técnicas, *Cargas para o cálculo de estruturas de edificações*, NBR 6120, 1980.

Author contributions: IDR: conceptualization, formal analysis, funding acquisition, methodology, writing original draft; GHFC, EMVP: funding acquisition, methodology, write-review & editing; LCMVJ, AL, GHS: project administration, supervision, write-review & editing.

Editors: Luis Oliveira Santos, Guilherme Aris Parsekian.